

MODELING OF DARK CURRENT GENERATION AND TRANSPORT USING THE IMPACT-T CODE*

J. Qiang[#], K. Hwang, LBNL, Berkeley, CA94720, U.S.A.

Abstract

Dark current from unwanted electrons in photoinjector can present significant danger to the accelerator operation by causing damage to photocathode and power deposition onto conducting wall. In this paper, we present numerical models of dark current generation from the field emission and from the electron impact ionization of the residual gas that were recently developed in the IMPACT-T code and a test application to the LCLS-II like injector.

INTRODUCTION

Dark current is normally referred as unwanted electrons in an accelerator. Those electrons lost onto photocathode, cavity wall or beam pipe can cause damage to the cathode material, increased heat load to superconducting surfaces, radioactivity beyond acceptable levels, and even other machine damage. It is one of limiting factors in the photoinjector design and operation, and has to be studied in these facilities [1-3]. In this paper, we report on the numerical modeling of the dark current generation and transport in a parallel beam dynamics code, IMPACT-T [4]. Here, the dark current includes two contributions: one is from the field emitted electrons, and another is from the electron impact ionization of the residual gas.

COMPUTATIONAL MODELS

We first present the numerical model for the dark current generation from the field emission electrons. The production of the dark current due to the field emission can be approximated using the Fowler-Nordheim equation [5]:

$$I = A_e \cdot 1.54 \cdot 10^{-6} \cdot 10^{4.52\phi - 0.5} \cdot \frac{\beta_0^2 E^2}{\phi} \cdot \exp\left(-\frac{6.53 \cdot 10^9 \phi^{1.5}}{\beta_0 E}\right) \cdot 1 \text{ A}$$

where \square is the enhancement factor of the electric field due to microscopic surface irregularities, A_e is the effective emitting area in units of m^2 , \square the work function of the material in units of eV, and E the macroscopic electric field applied to the material surface in units of V/m. Using the above equation and the time-dependent information of the electric field, we can obtain the time-dependent initial distribution of the dark current $I(t)$ in the tracking simulation. We assume that the electron are uniformly generated within the emitting surface area A_e with a Gaussian momentum distribution in a plane transverse to the surface normal direction, and a semi-Gaussian momentum distribution along the normal direction. These spatial coordinates and momenta are then transformed from the local coordinate system of the emitting surface to the global accelerator coordinate system for macroparticle tracking study.

*Work supported by the Director of the Office of Science of the US Department of Energy under Contract no. DEAC02-05CH11231.

[#]jqliang@lbl.gov

Another source of the dark current comes from the electron impact ionization of the residual gas, which can be important in a high average current injector. The electron beam colliding with the background residual gas can generate electrons through electron-impact ionization. Those electrons from the impact-ionization will be repelled by the space-charge forces of the electron beam and can move to large amplitude to become halo particles. The generation of these electrons can be simulated using a Monte Carlo method given a model for the impact-ionization probability of the residual gas. Here, the probability of production of an electron by the electron impact ionization during a time interval dt is given by [6]:

$$P_i = 1 - e^{-n_{\text{gas}}\sigma v dt}$$

where n_{gas} is the density of background residual gas, σ is the electron impact ionization cross-section, and v is the relative speed between the electron and the gas molecule. Given the ionization probability for an electron, a uniformly distributed random number r is generated. If $r < P_i$, then ionization occurs and an electron particle is generated. Once a dark current electron is generated, it will be subject to both the external forces of accelerating/focusing fields and the space-charge forces from the electron beam. The space-charge forces among the halo electrons and the space-charge forces on the main electron bunch due to the dark current electrons are neglected, given the fact that the number of these electrons is much less than the number of electrons in the main electron bunch. The initial spatial location of a dark current electron is assumed to be the same as that of the electron that produces the ionization. The initial velocity of the dark current electron is sampled from a Gaussian distribution with a given initial gas temperature.

APPLICATION TO A PHOTOINJECTOR

As a test of the dark current computational model in the IMPACT-T code, we simulated dark current generation and transport in an LCLS-II like photoinjector. The LCLS-II as a next generation high repetition rate x-ray free electron laser (FEL) light source is being actively studied [7-8]. The electron source for this accelerator comes from an injector that is schematically shown in Fig. 1 [9-10]. This injector consists of a 187 MHz low RF frequency photo-gun that accelerates an electron beam to about 750 keV, a solenoid magnet, a 1.3 GHz buncher cavity, another solenoid, and eight 1.3 GHz TESLA like superconducting cavities that accelerates the electron beam to about final 100 MeV energy. The designed repetition rate of the injector is 1 MHz with a plan to operate 20pC, 100pC and 300pC of electron charges.

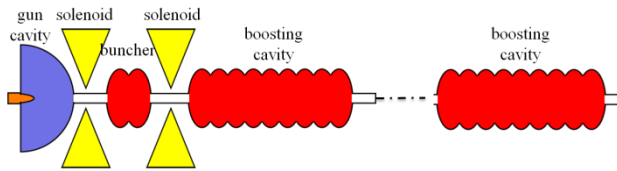


Figure1: A schematic plot of the LCLS-II injector layout.

Figure 2 shows the initial longitudinal current profile of the dark current from the field emission on the photocathode. Here we have assumed $A_c=1\mu\text{m}^2$, $\beta_c=60$, $\phi = 3\text{eV}$, and a sinusoid electric field on the photo-cathode with maximum amplitude $E_0 = 20\text{MV/m}$. The FWHM of the initial current distribution is about 0.4 ns. Using this initial current profile, we tracked dark current electrons emitted from a 1 mm by 1 mm square at the center of the cathode. Figure 3 shows the spatial distribution of these electrons inside the RF gun, buncher cavity, and first superconducting boosting cavity. It can be seen that the dark current beam transverse size blows up significantly inside the first boosting cavity. Such a large blow-up of transverse size in the first boosting cavity is also seen in Fig. 4, which shows the transverse maximum amplitude evolution of the dark current beam. This blow-up might be due to energy dependent RF focusing inside the cavity. The dark current electron coming into the cavity without a right phase and energy is defocused by the RF field. Figure 5 shows the longitudinal phase space (Z-E) and longitudinal-to-transverse phase space (Z-X) of the dark current beam at the exit of the injector. The longitudinal bunching through the 1.3 GHz boosting cavity is clearly seen from the phase space distribution. The dark current beam not only has a long energy tail but also has a large transverse amplitude. These large amplitude halo particles must be collimated downstream the accelerator before entering the FEL undulator.

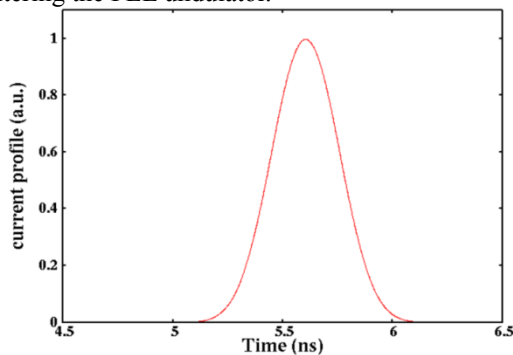


Figure 2: Field emitted dark current particle longitudinal distribution from the above Fowler-Nordheim equation.

Another source of the dark current is from the electron impact ionization of the residual gas. Using the Monte Carlo method discussed in the preceding section, we simulated the dark current generation and transport in the above LCLS-II like injector. Figure 6 shows the electron impact ionization cross section of several common residual gases (H_2 , H_2O , CH_4) as function of the electron

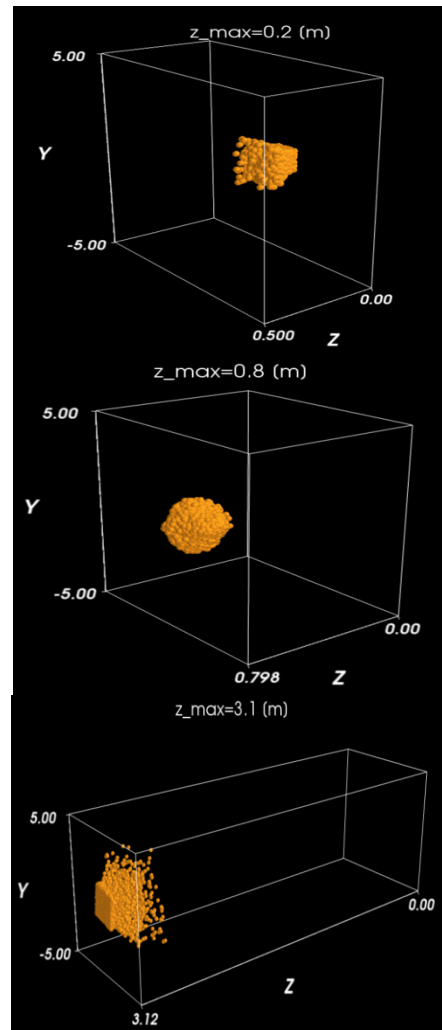


Figure 3: Dark current electron spatial distribution inside the VHF RF gun (top), bunch cavity (middle), and boosting cavity (bottom).

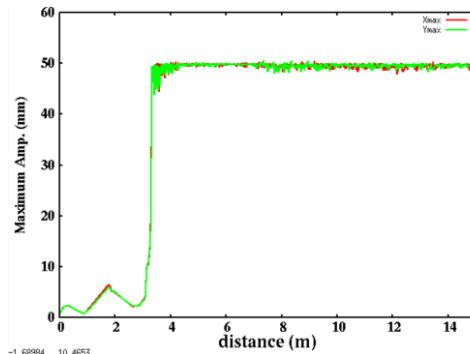


Figure 4: Maximum transverse size evolution of the field emitted dark current beam.

kinetic energy. It is seen that the maximum cross section for all those gases is below 100 eV.

The ionization cross section decreases by order of magnitude when the electron energy is beyond 10 keV. This suggests that the major electron ionization occurs inside the RF gun. Figure 7 shows the electron ionization dark current beam longitudinal phase space (Z-E) and longitudinal-to-transverse phase space (Z-X) after the

main electron bunch leaving the injector. Here, we have used 100pC charge for the main electron bunch following the nominal design of the LCLS-II. The effects of both the external field and the space-charge field from the main bunch are included in the tracking simulation of these dark electrons. It can be seen that the dark current beam has a very long low energy tail and very sharp high energy head. Only small fraction of the dark current electrons is accelerated together with the main bunch, the majority of the dark electrons is not accelerated and left with a very energy. From the plot of Z-X phase space plot, we can see that some of those low energy dark electrons have large transverse amplitude and can be lost inside the injector. In this test study, only one residual gas species (H2) is used with a pressure 5×10^{-5} Torr. This large pressure is used to increase the numerical resolution in the dark current particle distribution.

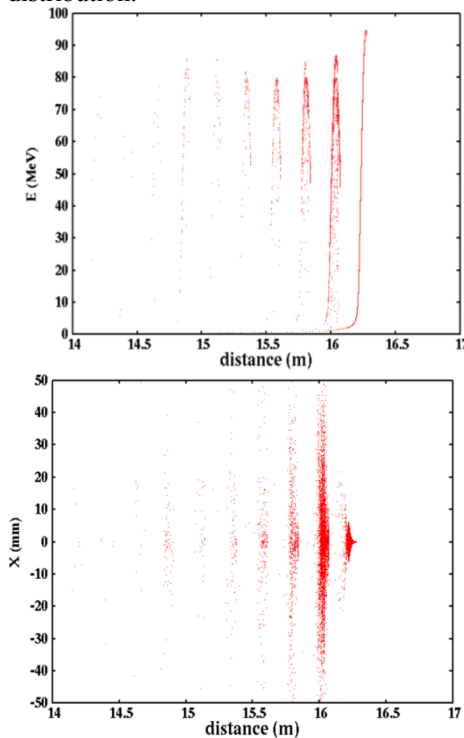


Figure 5: Longitudinal phase space (top) and longitudinal to transverse phase space (bottom) of the dark current beam at the exit of the injector.

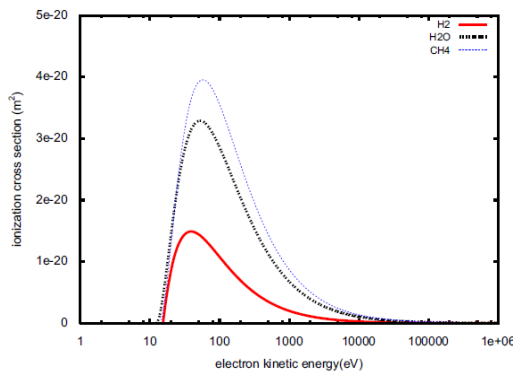


Figure 6: Electron impact ionization cross section of several gases as a function of electron kinetic energy.

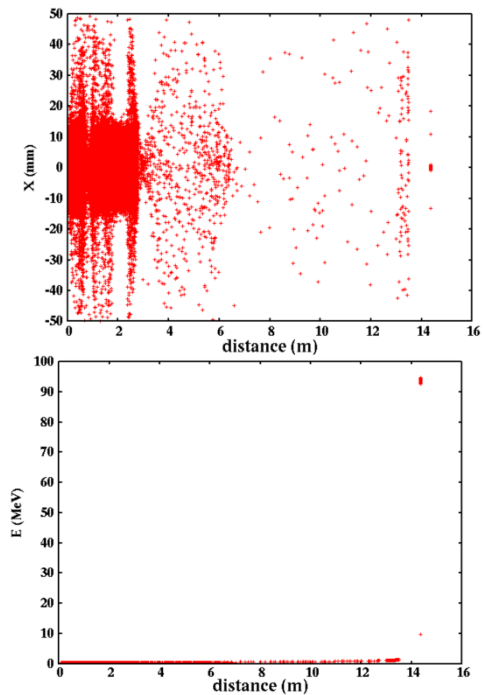


Figure 7: Longitudinal phase space (top) and longitudinal to transverse phase space (bottom) of the electron ionization dark current beam at the exit of the injector.

ACKNOWLEDGEMENT

We would like to thank the LCLS-II injector design team for the injector parameters used in this test study.

REFERENCES

- [1] J. Han *et al.*, *Phys. Rev. ST-Accel. Beams*, vol. 11, p. 013501, 2008.
- [2] R. Xiang *et al.*, *Phys. Rev. ST-Accel. Beams*, vol. 17, p. 043401, 2014.
- [3] R. Huang *et al.*, *Phys. Rev. ST-Accel. Beams*, vol. 18, p. 013401, 2015.
- [4] J. Qiang *et al.*, *PRST-AB* 9, 044204 (2006).
- [5] R. Fowler and L. Nordheim, *Proc. R. Soc. A*, vol. 119, 173 (1928).
- [6] J. Wang, P. Liewer, E. Huang, *J. Supercomputing*, vol. 10, p. 331, 1997.
- [7] T. O. Raubenheimer, in *Proc. IPAC2015*, Richmond, VA, USA, May 2015, paper WEYC1.
- [8] P. Emma *et al.*, in *Proc. FEL'14*, paper THP025, p. 473.
- [9] J. F. Schmerge *et al.*, in *Proc. FEL14*, Basel, Switzerland, 2014, p. 815.
- [10] F. Zhou *et al.*, in *Proc. FEL15*, Daejeon, Korea, 2015, p. 78.